**Electronic Supplementary information**

**for**

# Enhanced $H_2$ production assisted by anodic iodide oxidation using transparent tin oxide-based electrodes

**Table of Contents**


| S. No | Contents | Page no. |
|---|---|---|
| 1 | Chemicals | S3 |
| 2 | Cleaning of FTO and ITO electrodes | S3 |
| 3 | Characterization details | S3 |
| 4 | Electrochemical measurement details | S4 |
| 5 | Product Quantification details | S5-S6 |
| 6 | Fig. S1 XRD pattern of FTO and ITO | S7 |
| 7 | Fig. S2 Raman spectrum of FTO and ITO | S8 |
| 8 | Fig. S3 FESEM images of FTO and ITO | S9 |
| 9 | Fig. S4 LSVs of IOR with lower concentrations of NaI | S9 |
| 10 | Fig. S5 Effect of pre-treatment of FTO on IOR activity | S10 |
| 11 | Fig. S6 LSVs and Nyquist plot of FTO and ITO for IOR | S10 |
| 12 | Fig. S7 Bode plot of FTO electrode for OER and IOR | S11 |
| 13 | Fig. S8 Digital photograph of H-cell 3 electrode setup | S12 |
| 14 | Fig. S9 UV-Vis spectra of iodine standards and calibration curve | S13 |
| 15 | Fig. S10 Details of extraction of $I_2$ and corresponding UV-Vis spectra | S14 |
| 16 | Fig. S11 Long-term chronopotentiometry test at 10 mA/cm$^2$ | S15 |
| 17 | Fig. S12 XRD patterns before and after long term chronopotentiometry test | S16 |
| 18 | Fig. S13 Raman spectra before and after long term chronopotentiometry test | S16 |
| 19 | Fig. S14 FESEM images and EDS data after long term chronopotentiometry test | S17 |
| 20 | Fig. S15 XPS spectra before and after long term chronopotentiometry test | S18 |
| 21 | Fig. S16 FESEM images and Mott-Schottky data after long term chronopotentiometry test | S19 |
| 22 | Fig. S17 Chronoamperometry test for 22 h | S20 |
| 23 | Fig. S18 Scheme showing the liquid products obtained during IOR carried out with and without applied voltage. | S21 |
| 24 | Fig. S19 LSVs recorded in 0.1 M $Na_2SO_4$ | S21 |
| 25 | Fig. S20 Concentration dependant polarization curves recorded in 2-electrode electrolyzer | S22 |

| | | |
|---|---|---|
| 26 | Fig. S21 Gas chromatograms for the sample collected from hybrid and traditional water electrolysis cells. | S22 |
| 21 | Comparison Table-1 | S23 |
| 22 | Comparison Table-2 | S24 |


## 1. Experimental Section

### 1.1 Chemicals

Sodium hydroxide (NaOH, Loba Chemie, 97%), Ethanol ($C_2H_5OH$, Fischer Scientific, 99.9%), Acetone ($C_3H_6O$, Fischer Scientific, 99%), Sodium Iodide (NaI, Loba Chemie, 99%), Perchloric acid ($HClO_4$, Fischer Scientific, 97%), Sodium sulphate ($Na_2SO_4$, Loba Chemie, 99%). All chemicals were used as-received. Aqueous solutions were prepared using deionised (DI) water (Resistivity = 18.3 MΩ). Transparent conductive oxides (TCO) namely Fluorine doped tin oxide (FTO) (thickness: 1.6 mm, thickness of conductive layer: ~500 nm, resistivity: 7 ohm/sq) and indium tin oxide (ITO) (thickness: 0.7 mm, thickness of conductive layer: 180-200 nm, resistivity: 10 ohm/sq) coated glass substrates were purchased from Sigma Aldrich and Techinstro, respectively.

### 1.2 Cleaning of FTO and ITO electrodes

Prior to electrochemical measurements, the FTO and ITO coated glass substrates were cut into required dimensions and were subsequently cleaned by sonicating 10 min. each in acetone, in ethanol and in water sequentially.[1] After cleaning, the substrates were dried under ambient conditions, before use.

### 1.3 Characterization

Powder XRD patterns were obtained using X-ray diffractometer (Bruker D8 Advance) in the 2θ range of 5 to 90° at a scan rate 3.5 °/min with Cu-Kα radiation (λ = 1.5405 Å). Raman spectra were obtained using LabRAM, Horiba Jobin Yvon Raman microscope with an excitation wavelength of 532 nm. Morphology of the FTO/ITO coated glass substrates was examined

using field emission-scanning electron microscope (Quanta FEG250, FEI) (FESEM) equipped with energy dispersive X-ray (EDX) analysis. X-ray photoelectron spectroscopy (XPS) measurements were carried out using K-alpha, Thermo Fischer instrument with an Al Kα X-ray source (1486.6 eV). UV-visible spectrophotometer (Jasco V-770) was used to detect the liquid oxidation product. To quantify $H_2$, Gas chromatograph (Agilent 8890) equipped with Molsieve 5A 80/100 SS packed column and a thermal conductivity detector (TCD) was used.

**1.4 Electrochemical measurements**

Pre-cleaned TCO electrodes were used as working electrodes in electrochemical studies. Electrochemical tests were performed in custom-built electrochemical cells using electrochemical workstation (SP150e, Biologic). Preliminary electrochemical measurements were carried out in three-electrode setup, wherein, FTO or ITO were used as working electrode (WE), graphite rod was used as the counter electrode (CE) and saturated calomel electrode ($Hg/Hg_2Cl_2$/Sat. KCl) (SCE) was used as the reference electrode. Polarization curves were recorded in 0.1 M $HClO_4$ for oxygen evolution reaction (OER) and in 0.1 M $HClO_4$ with known concentration of NaI for iodide oxidation reaction (IOR) at a scan rate of 5 mV/s. Prior to the measurements, the electrolyte was de-aerated by purging with high pure Ar gas. The electrochemical cells were isolated from stray light exposure by covering them with aluminium foil during the measurements. The measured potential vs. SCE was converted into reversible hydrogen electrode (RHE) using the following equation (equation 1),

$$E_{RHE} = E_{MMO} + E^{o}_{SCE} + 0.059 \times pH \qquad (1)$$

where $E^{o}_{SCE}$ is standard potential of SCE (0.241 V vs. NHE).[2]

Electrochemical impedance spectroscopic (EIS) measurements were performed at the onset potential over a frequency ranging from 10 kHz to 0.1 Hz at an amplitude of 5 mV. For potential dependent EIS, measurements were done from 1.65 V vs RHE to 2.15 V vs RHE for OER and

from 0.65 V vs RHE to 1.20 V vs RHE for IOR in a frequency ranging from 10 kHz to 0.1 Hz at an amplitude of 5 mV.

The two-electrode electrochemical measurements were carried out using custom-build two compartment H-cell setup in which Pt-wire was employed as the cathode (for HER) and FTO coated glass substrate served as the anode (for IOR). Nafion$^{TM}$ 211 proton exchange membrane was used as the separator. The capacity of each compartment in the H-cell is 60 mL. The anode compartment contains 30 mL of 1 M NaI in 0.1 M $HClO_4$ while the cathode compartment was filled with 30 mL of 0.5 M $H_2SO_4$.

All polarization curves were iR-corrected (80 %) (equation 2) unless otherwise stated.

$$E_{iR\ corrected} = E_{measured} - i \times R_s \qquad (2)$$

$E_{measured}$ is the experimentally measured potential, and $R_s$ is the solution resistance obtained from EIS measurements.

**1.5 Product Quantification**

Product quantification studies were carried out in H-type electrochemical cells in 3-electrode as well as 2-electrode configurations.

Quantification of liquid products:

The product formed during IOR under potentiostatic test was determined both qualitatively and quantitatively. The electrode obtained after long term stability was characterized using XPS and FESEM-EDS to qualitatively determine the presence of I-species adsorbed on the surface. The quantification of iodine (as $I_3^-$) was performed using UV-visible spectroscopy measurements. The iodine formed during IOR present as $I_3^-$, which is known to absorb at 350 nm. Known amounts of aliquots collected at different time intervals from the cell were diluted before collecting absorption spectra. Calibration plot obtained by recording absorbance at 350

nm (corresponding to absorbance of $I_3^-$) from various standard solutions, was used to estimate the amount of the product formed during electrochemical oxidation of iodide.

The anodic oxidation product obtained after long-term tests (22 h.) carried out at 1.17 V vs RHE using chronoamperometry was also quantified by collecting 100 µL aliquot of the sample that was added to 14.9 mL water (total volume 15 mL), prior to absorbance measurements.

To confirm the $I_2$ formed during the IOR process, extraction of the electrolyte was done in chloroform due to higher solubility of $I_2$ in chloroform. The mixtures were left to separate into two phases, as shown in Fig. S10a. The bottom layer (containing $I_2$) was carefully collected in a flask. This procedure was repeated until the top and bottom layers become colourless, indicating that all the $I_2$ has been extracted from the electrolyte. The extracted $I_2$ is shown in the inset of fig. S10b (top).

Quantification of gaseous products ($H_2$):

The $H_2$ gas generated during the course of the reaction was quantified by collecting the gases from the headspace of CE compartment (for 3-electrode setup) and from the cathode compartment (for 2-electrode setup) using airtight Hamilton syringes. The gases (200 µL) were injected into GC equipped with TCD detector.

Faradaic efficiency (%FE) for $H_2$ and $I_2$ ($I_3^-$) was calculated using the following equation,

$$\% FE = \frac{n \times mole\ of\ product formed \times F}{Total\ charge\ passed} \times 100\ \% \qquad (3)$$

where n is the number of transferred electrons, n=2 for $H_2$ evolution and n=2 for $I_2(I_3^-)$ evolution and F is the Faraday constant (96,485 C $mol^{-1}$).

Energy-saving efficiency ($\eta$) at a given current density is calculated using the following equation[3],

$$\eta = \frac{(Cell\ voltage\ of\ the\ OER - Cell\ Voltage\ of\ the\ IOR)}{(Cell\ voltage\ of\ the\ OER)} \times 100 \qquad (4)$$

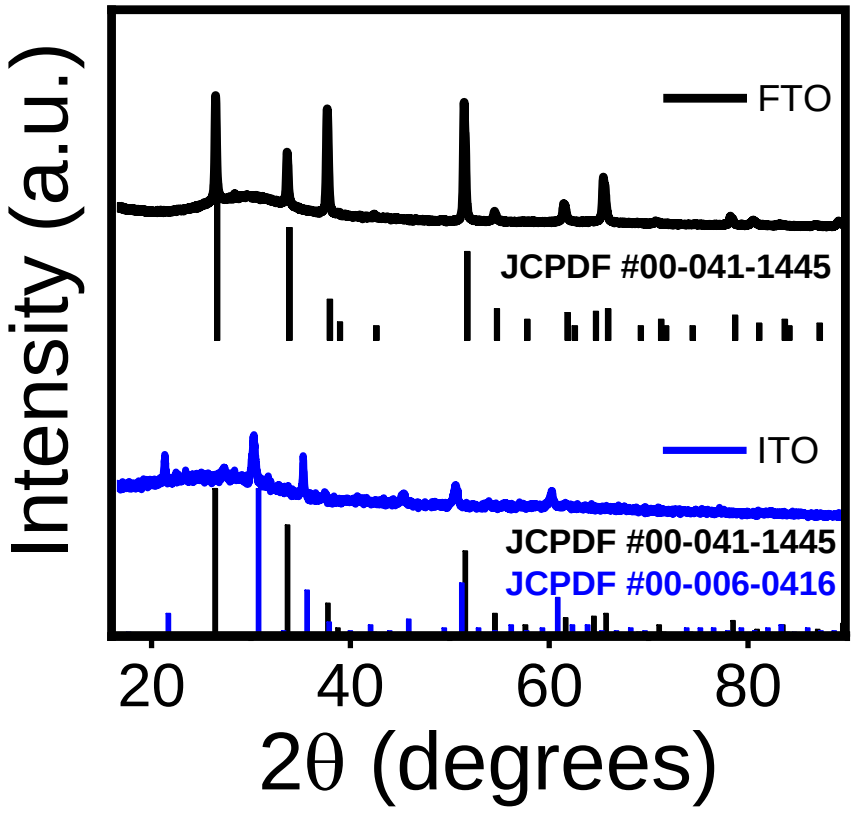


Fig. S1 XRD patterns of commercial FTO and ITO coated glass substrates.

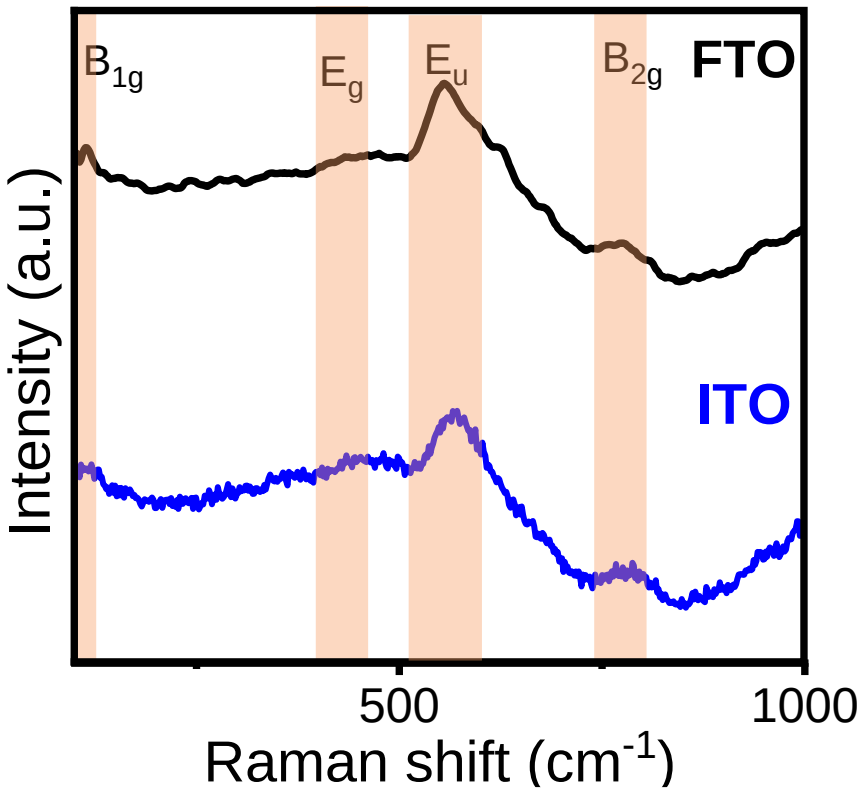


Fig. S2 Raman spectra of commercial FTO and ITO coated glass substrates recorded using 532 nm laser as excitation source.

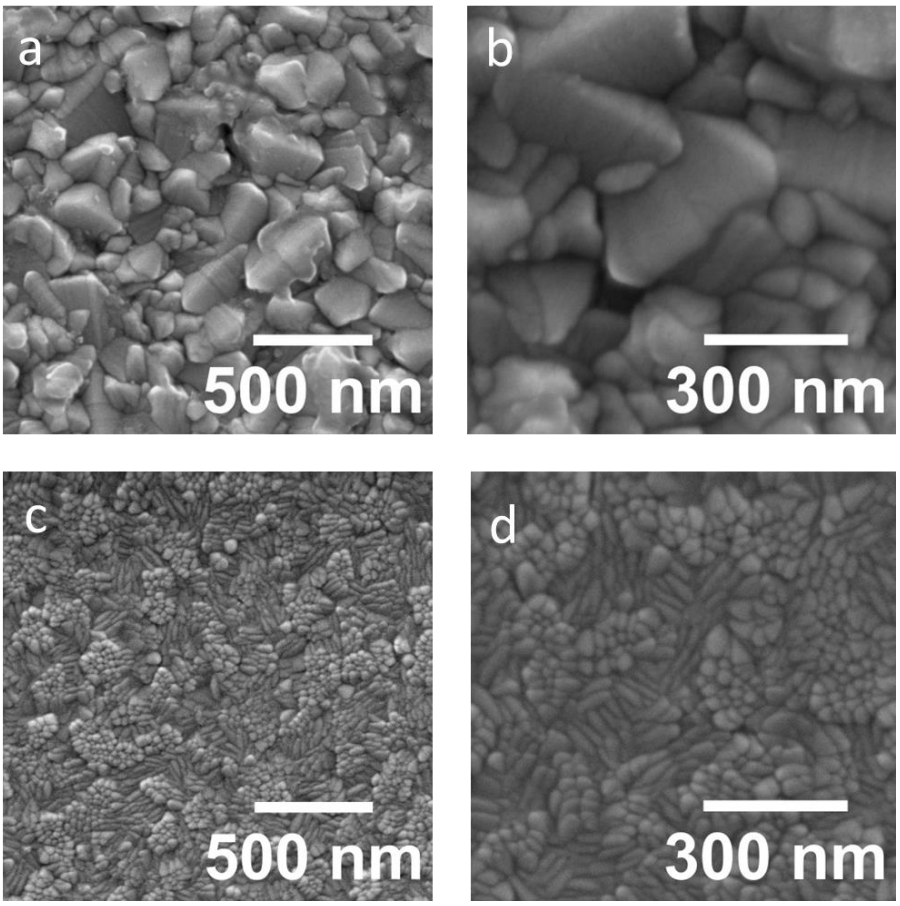


Fig. S3 FESEM images of freshly cleaned FTO (a & b) and ITO (c & d) coated glass electrodes

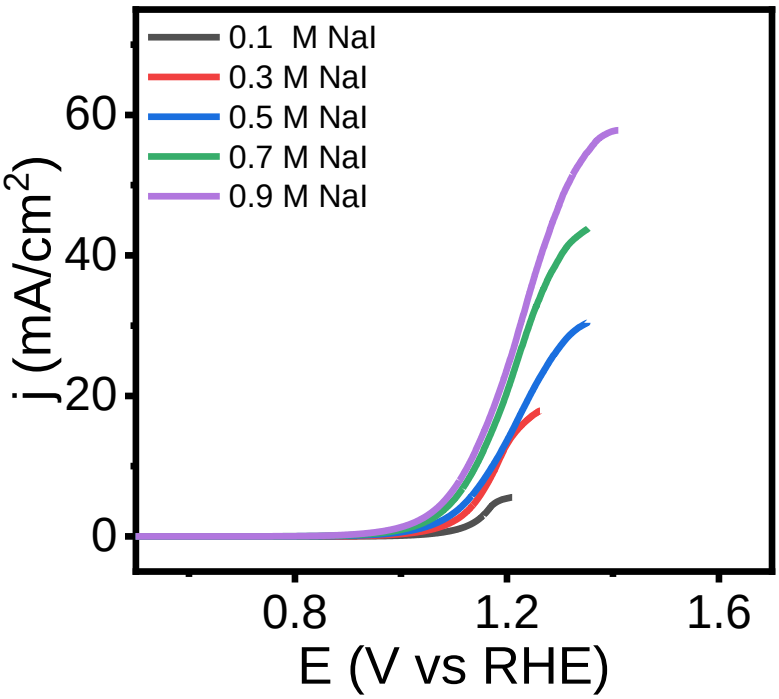


Fig. S4 Linear sweep voltammograms depicting the variation of IOR activity with concentration of NaI in 0.1 M $HClO_4$ at 5 mV/s.

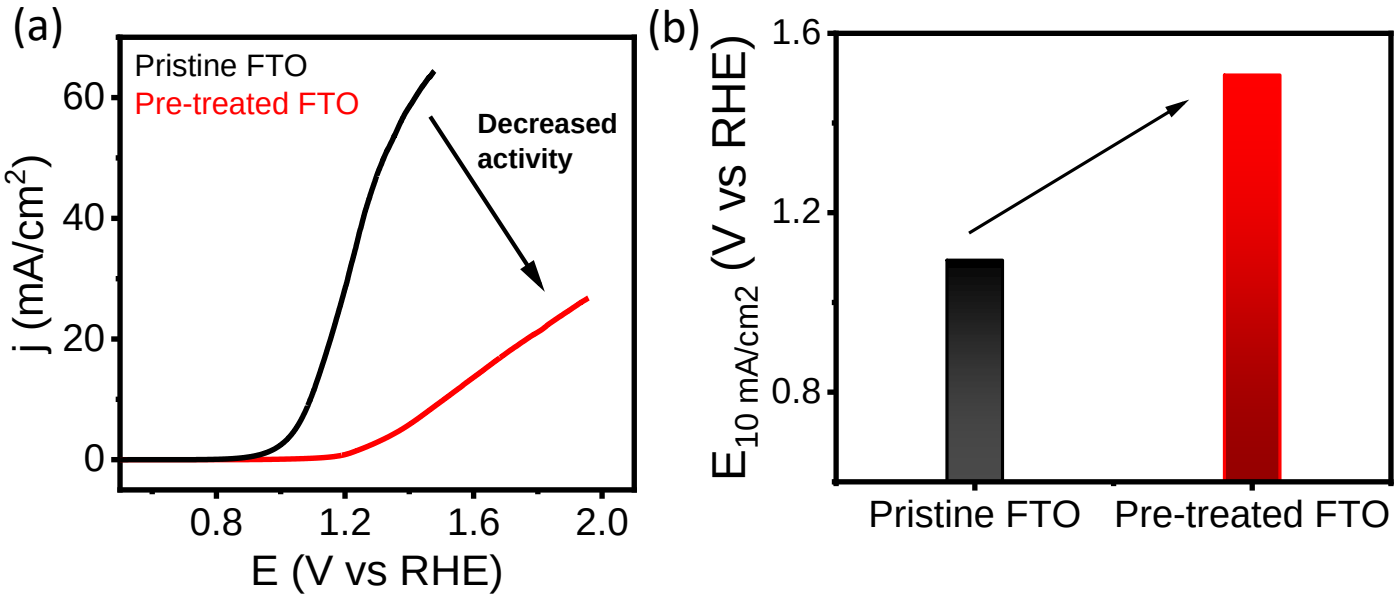


Fig. S5 (a) Linear sweep voltammograms recorded for IOR using pristine FTO (no pre-treatment) and pre-treated FTO at 5 mV/s in 0.1 M $HClO_4$ with 1 M NaI, (b) corresponding bar plot depicting potential at 10 mA/cm$^2$ obtained for pristine and pre-treated FTO. The pre-treatment procedure: Chronoamperometry at 3.3 V vs RHE for 10 min.

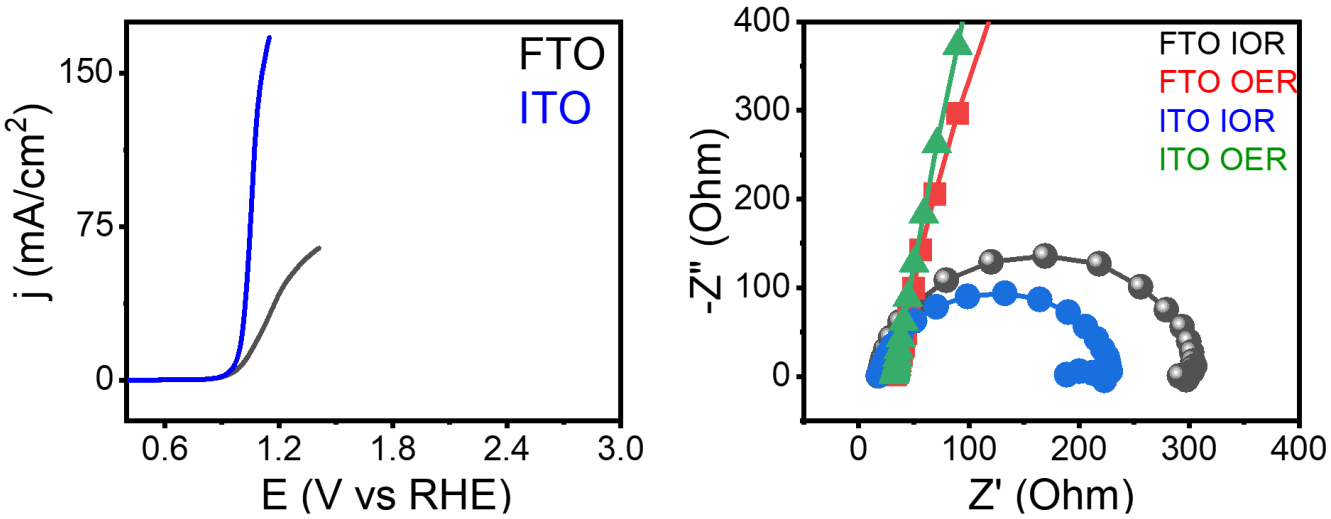


Fig. S6 (a) Linear sweep polarisation curves showing IOR recorded using FTO and ITO electrodes at 5 mV/s, (b) EIS data for OER and IOR recorded at onset potentials using FTO, ITO electrodes.

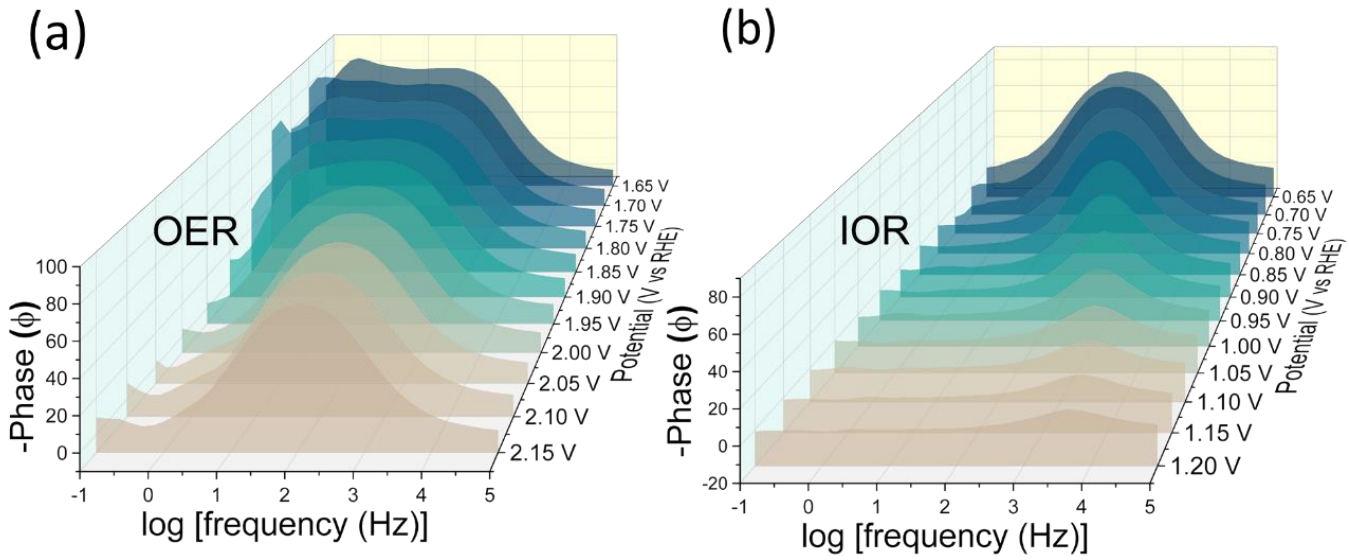


Fig. S7 Bode phase plots obtained from *in-situ* electrochemical impedance spectroscopy measurements recorded at various potentials in (a) absence and (b) presence of 1 M NaI, in 0.1 M $HClO_4$.

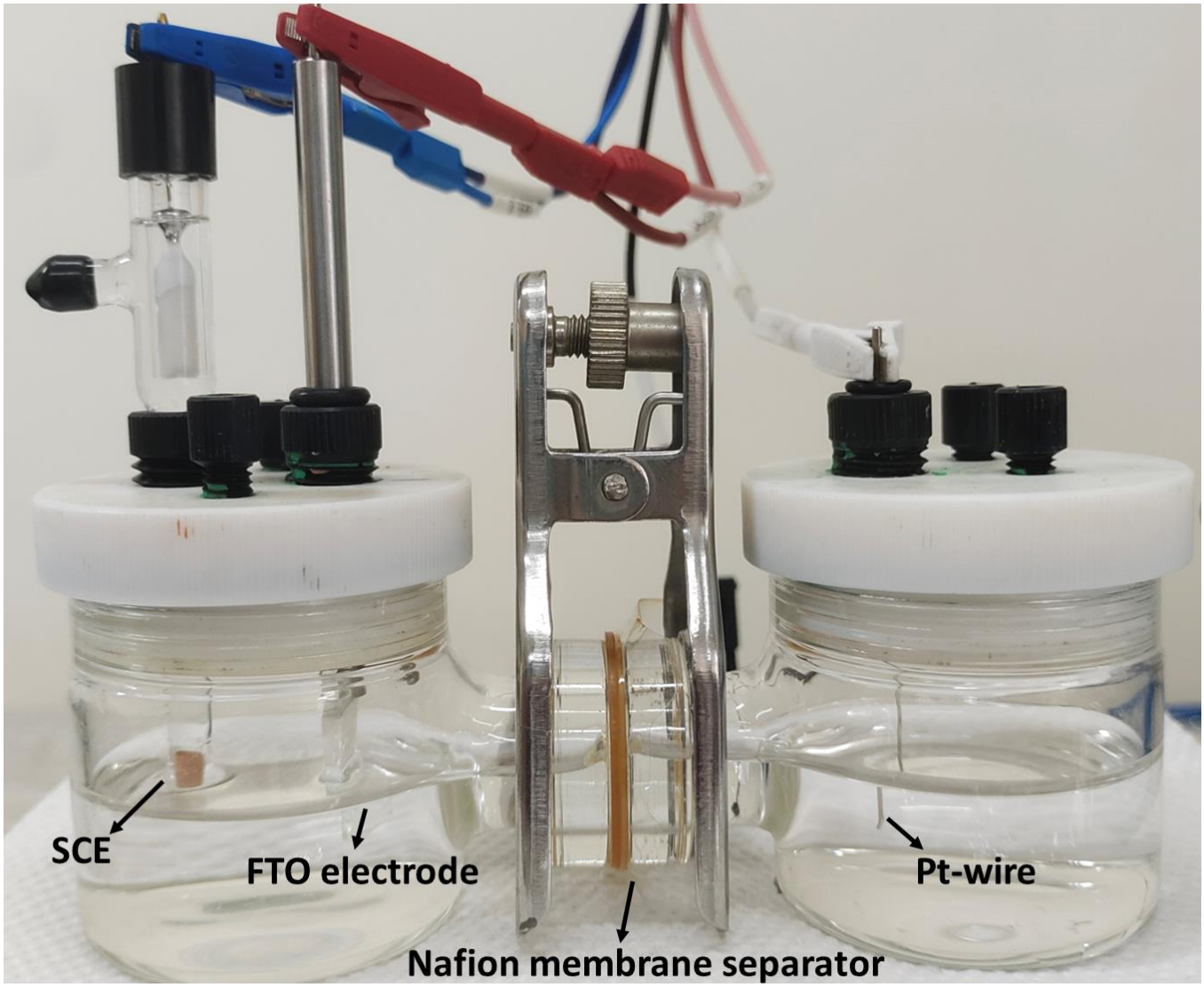


Fig S8. Digital photograph of H-type cell setup used in the present study.

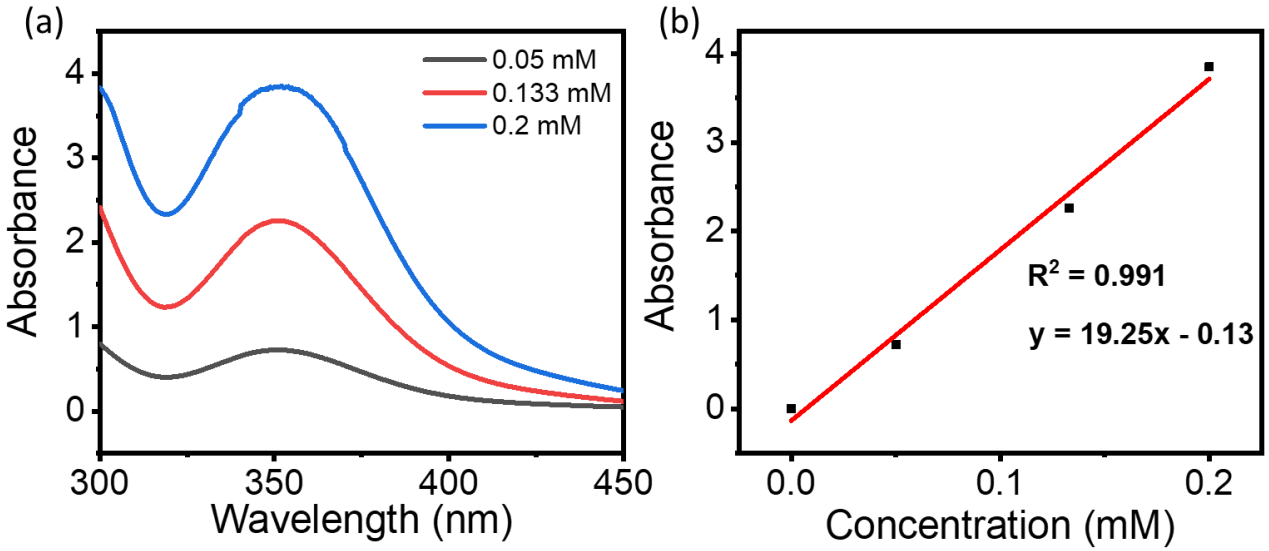


Fig. S9 (a) UV-vis absorption spectra of various concentrations of standard $I_2$ (in $I^-$) and (b) Calibration plot depicting variation of absorbance at 350 nm (corresponding to $I_3^-$) with change in concentration.

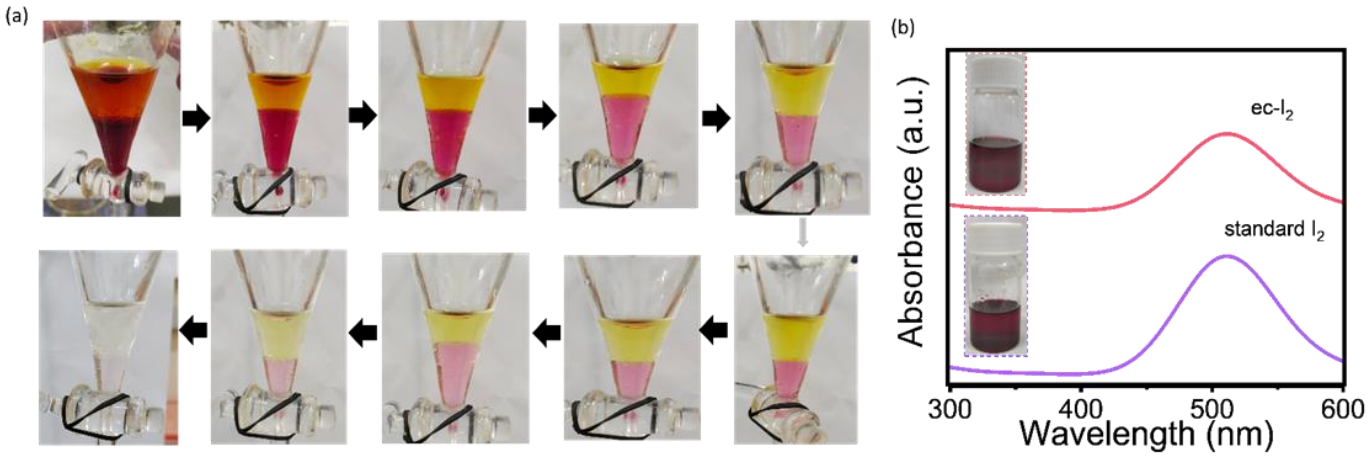


Fig. S10 (a) Digital photographs depicting different stages of extraction of $I_2$ in chloroform from the reaction mixture collected after long-term electrochemical test, (b) UV-Visible spectra of standard $I_2$ (20 mM) and electrochemically generated $I_2$. Inset: Standard $I_2$ (bottom) and electrochemically produced $I_2$ (extracted) product after separation (top). The ec-$I_2$ in Fig. (b) represents electrochemically produced $I_2$.

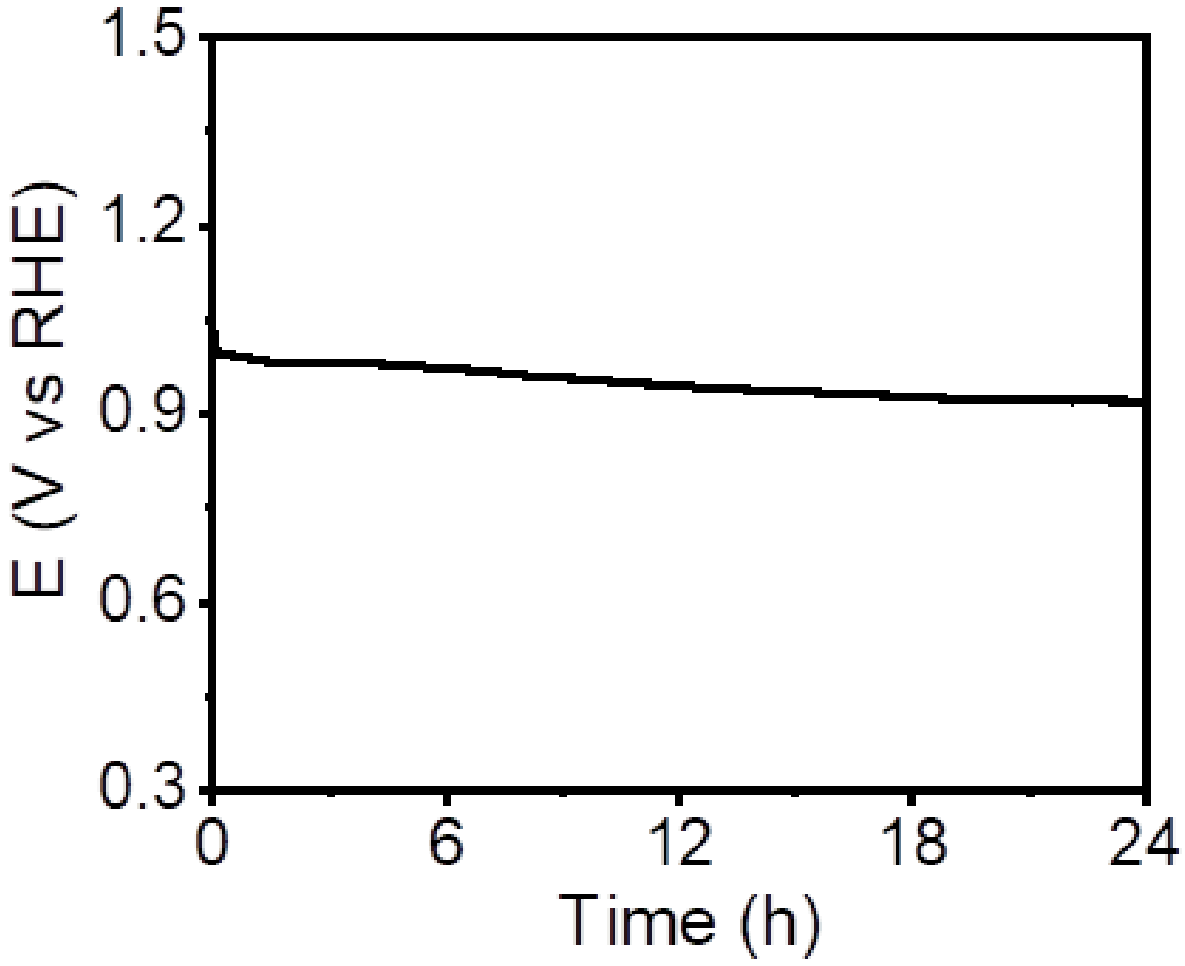


Fig. S11 Chronopotentiometry measurement performed using FTO electrode when the system is held at 10 mA/cm$^2$ for the duration of 24 h.

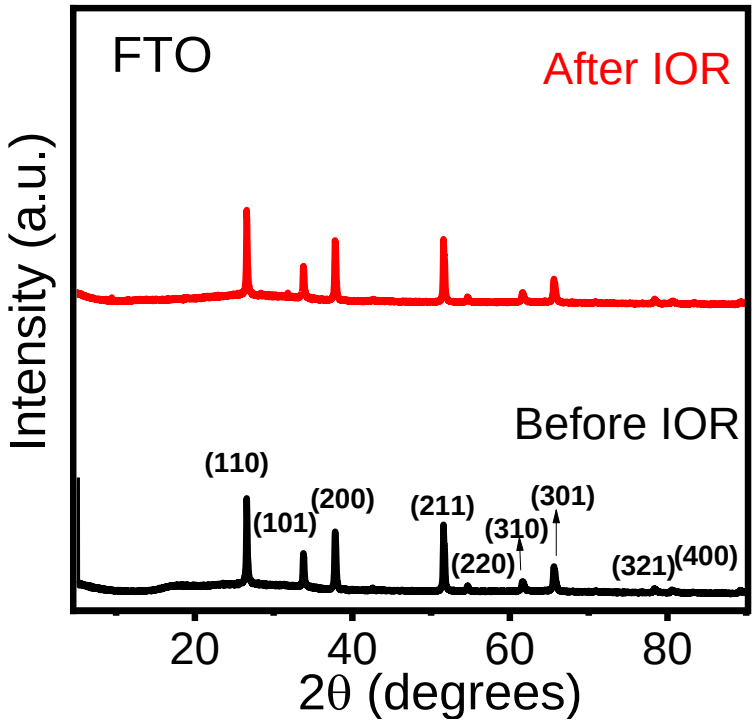


Fig. S12 XRD patterns of FTO electrode before and after long term chronopotentiometry test at 10 mA/cm$^2$ for 24 h.

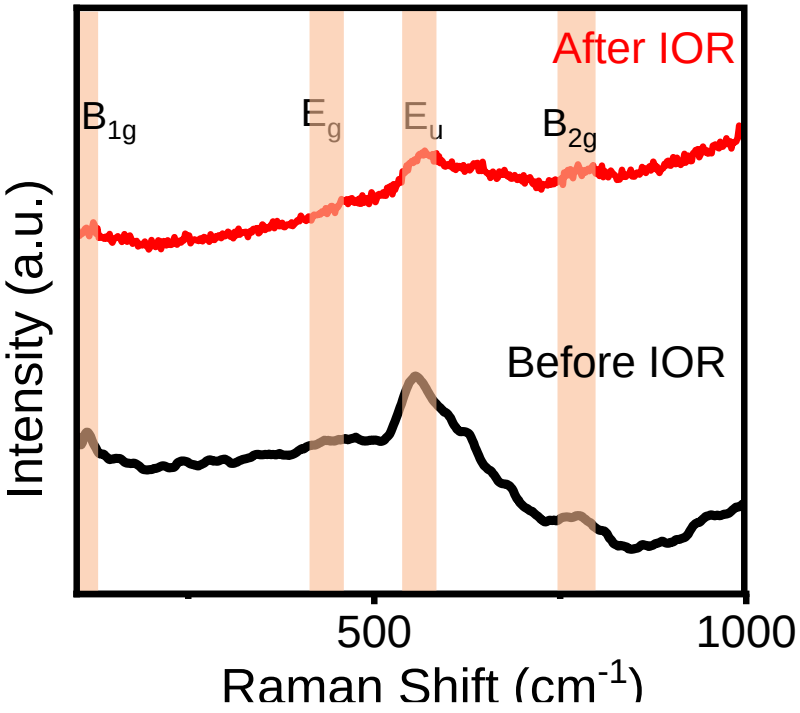


Fig. S13 Raman spectra of FTO electrode recorded before and after long term chronopotentiometry test at 10 mA/cm$^2$ for 24 h.

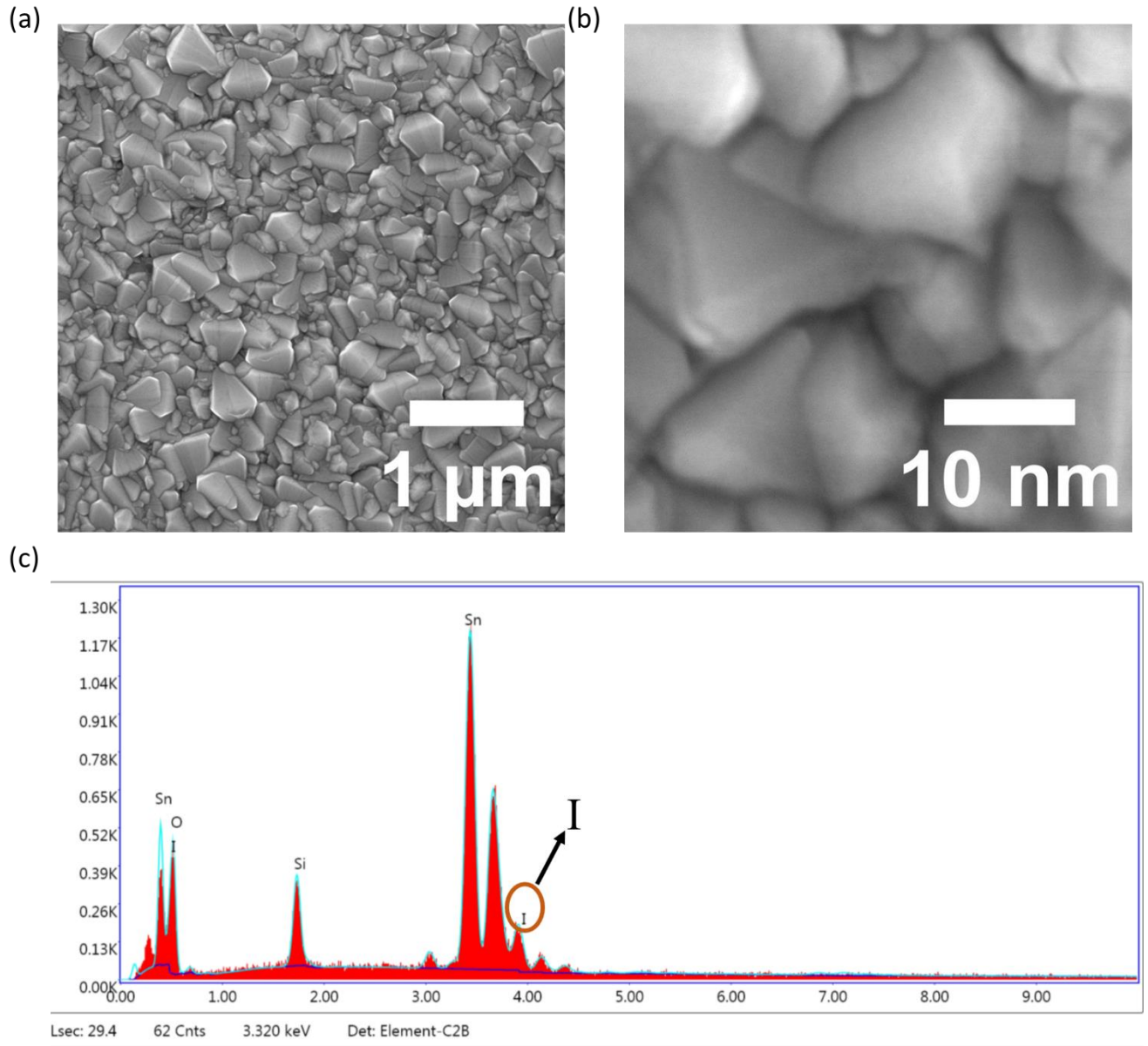


Fig. S14 (a), (b) represent FESEM images and (c) EDS of FTO electrode after long term chronopotentiometry test.

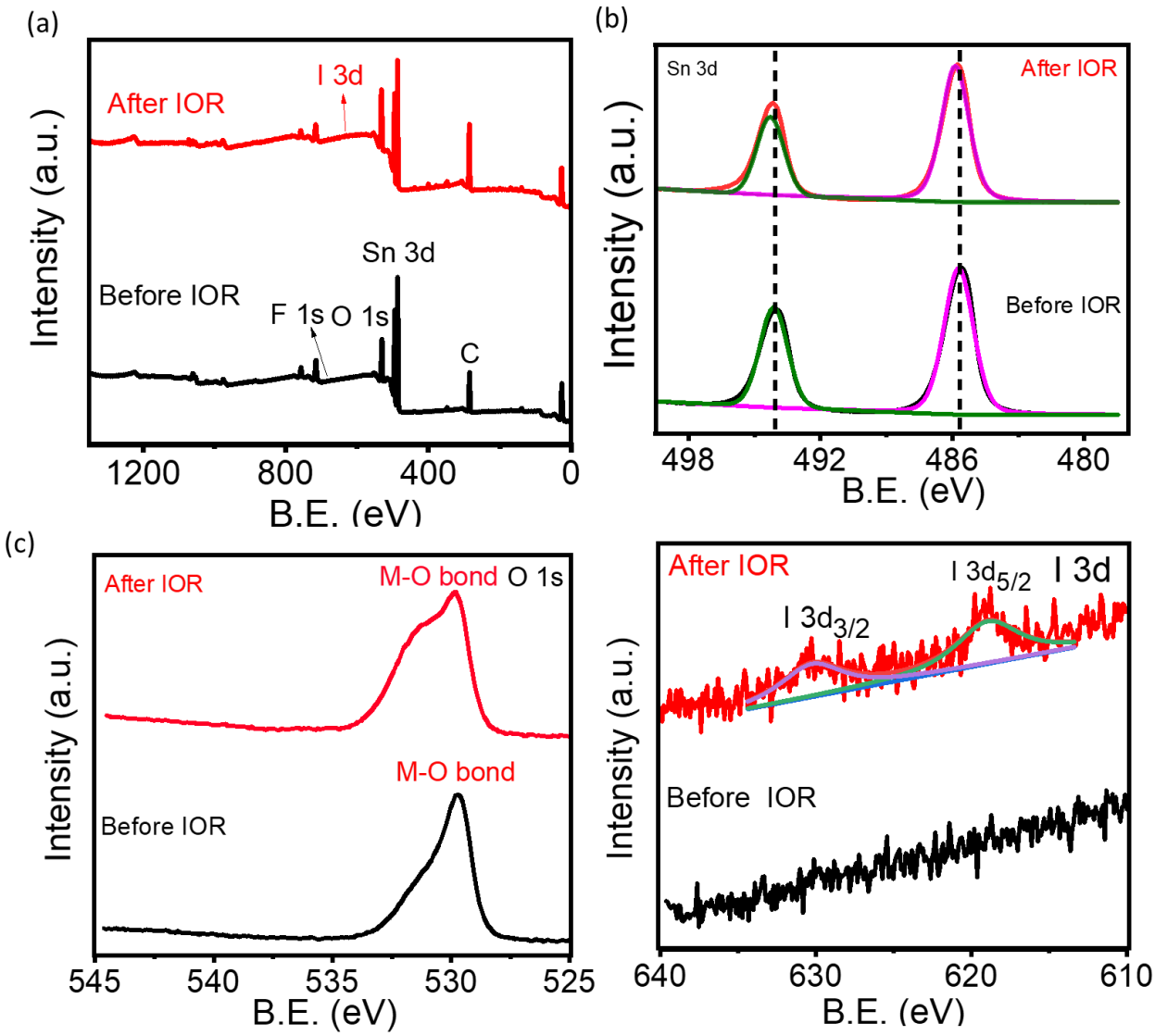


Fig. S15. XPS (a) survey spectra, core-level spectra of (b) Sn 3d (c) O 1s, (d) I 3d regions, of FTO electrode recorded before and after long term chronopotentiometry test performed at 10 $mA/cm^2$ for 24 h.

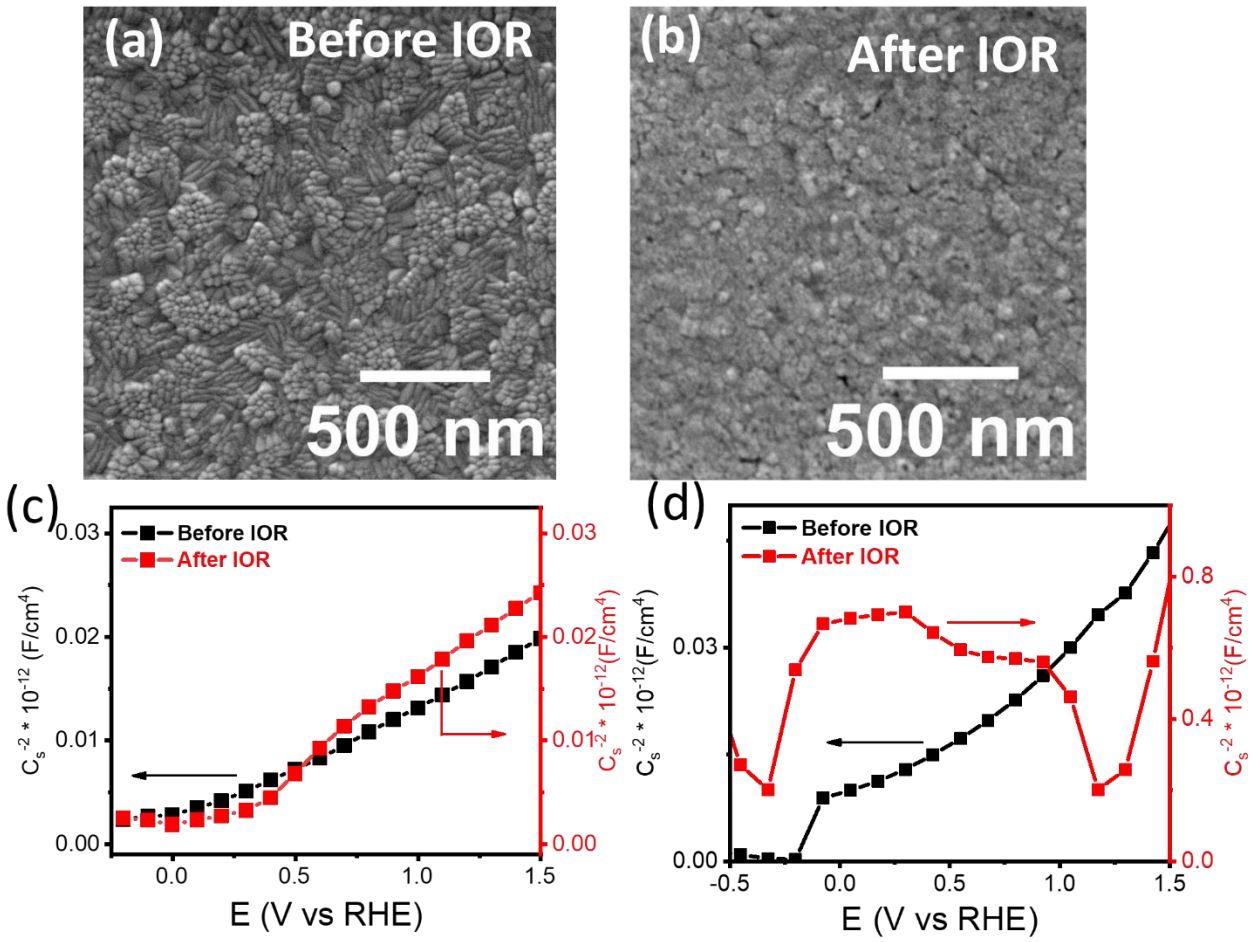


Fig. S16 FESEM images of ITO (a) before and (b) after long-term stability test, Mott-Schottky plot of (c) FTO and (d) ITO electrode before and after long-term chronopotentiometry test at 10 mA/cm$^2$ for 22 h. recorded at 1000 Hz.

The stability of ITO electrode obtained after long-term stability measurements performed at 10 mA/cm$^2$ for 22 h. in acidic medium is studied in greater detail. The ITO electrode after long-term stability tests were characterized using techniques like field emission scanning electron microscopy (FESEM), and Mott-Schottky measurements. As shown in Fig. S16a and S16b of the revised ESI, an evident change in the morphology of ITO of post-catalysis is noted when compared to ITO of pre-catalysis, suggesting that ITO is not stable unlike the FTO which shows similar morphology even after long-term stability tests. (FESEM images of FTO before and after long-term stability test are already given as Figs. S14a & S14b in the ESI). In order to further understand the stability of TCOs, Mott-Schottky (M-S) measurements were performed for both FTO and ITO (Fig. S16c and S16d) electrodes before and after the long-term tests. As evident from the Fig. S16c, the FTO shows negligible changes in M-S data of FTO before and after long-term tests, suggesting the robustness of FTO. However, the M-S data of ITO before long-term tests is significantly different from that of ITO after long-term tests (Fig. S16d),

indicative of considerable changes in the ITO surface during IOR process. All these measurements suggest that the FTO is relatively more stable than ITO.

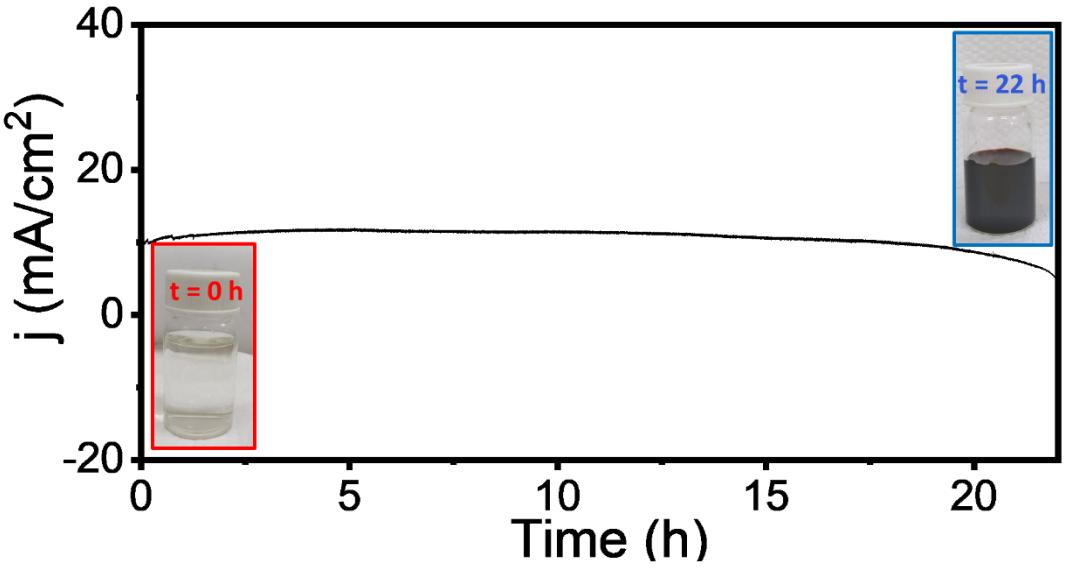


Fig. S17. Chronoamperometry recorded in 1 M NaI in 0.1 M $HClO_4$ using FTO electrode at an applied potential of 1.17 V vs RHE. The digital pictures given as insets represent the electrolyte before and after the electrochemical oxidation of $I^-$.

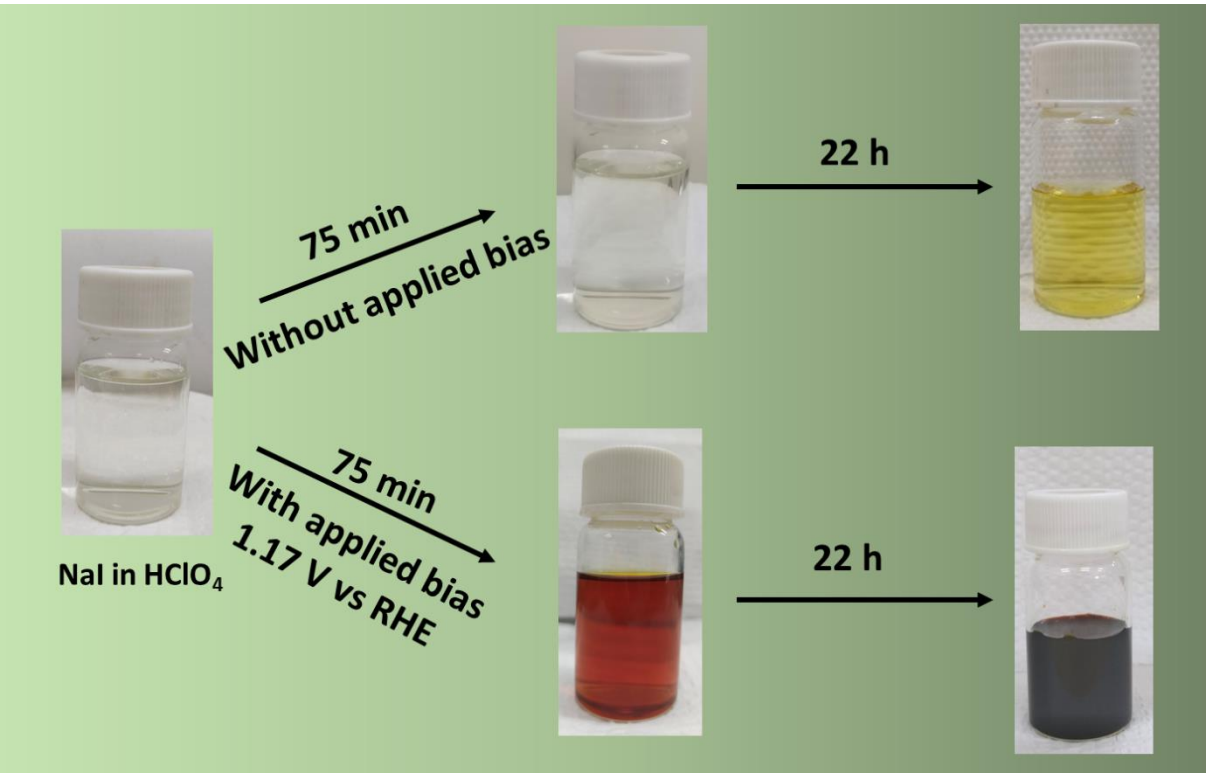


Fig. S18 Schematic illustration of the oxidation of iodide performed with and without application of voltage.

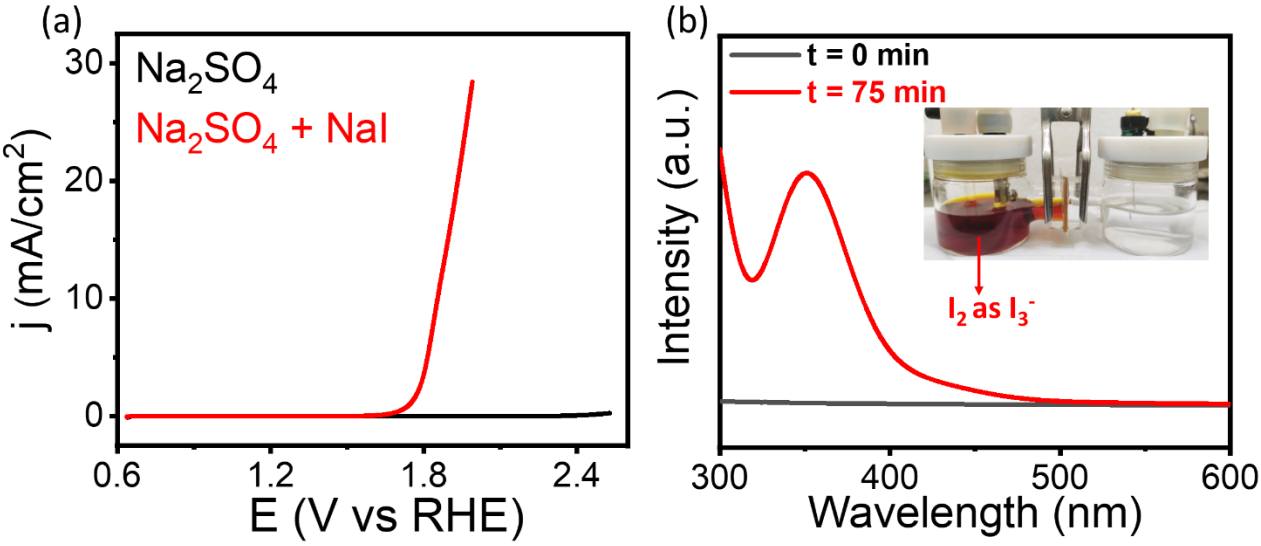


Fig. S19 (a) *iR*-corrected linear sweep voltammograms obtained using FTO with and without 1 M NaI in 0.1 M $Na_2SO_4$, (b) UV-visible spectra of the electrolyte (diluted) collected at t=0 min. and t=75 min. when the IOR experiment was carried out at 1.86 V vs RHE in 0.1 M $Na_2SO_4$ with 1 M NaI. Inset represent digital picture captured after 75 min. of the reaction neutral medium.

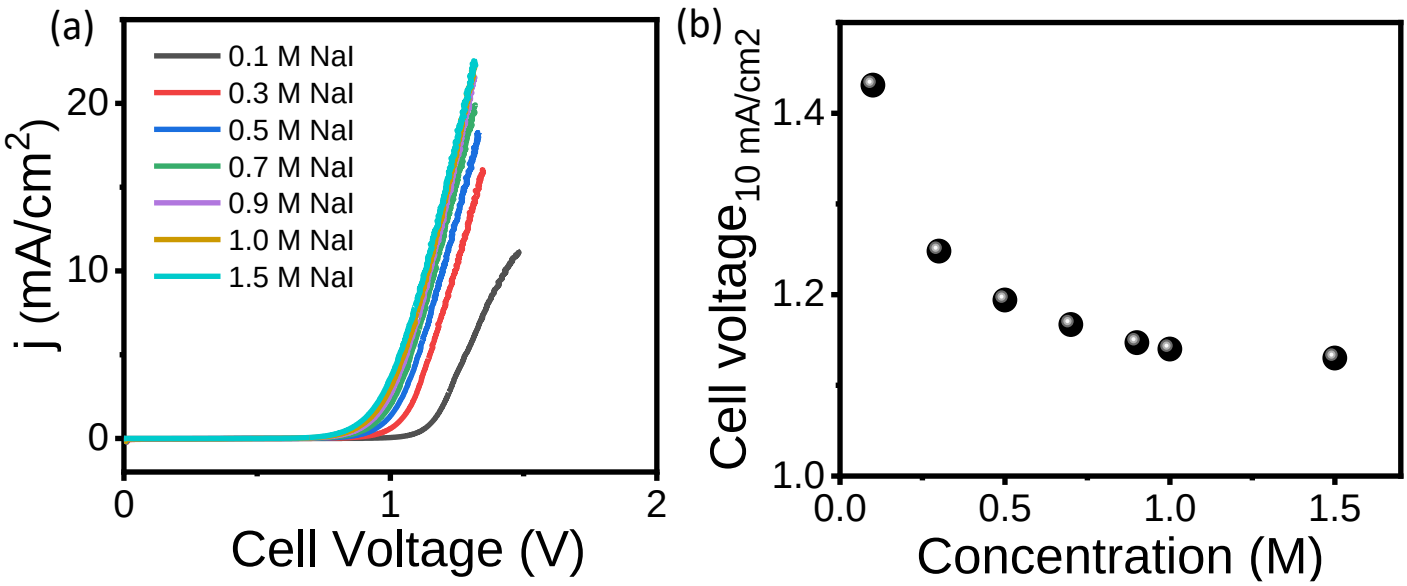


Fig. S20 (a) depicts the variation of voltammograms with concentration of NaI for hybrid water electrolysis cell (IOR||HER) consisting of FTO as anode and Pt-wire as cathode recorded in 0.1 M $HClO_4$ at 5 mV/s, (b) variation of cell voltage at 10 $mA/cm^2$ with concentration of NaI.

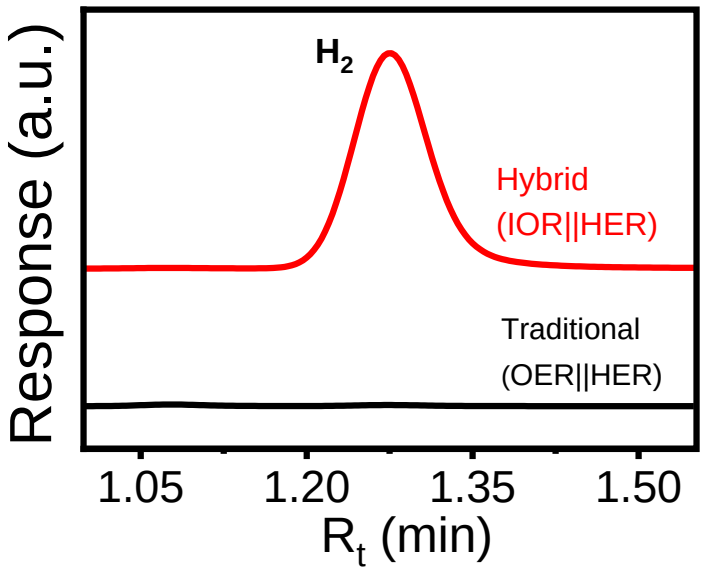


Fig. S21 Gas chromatograms recorded for the gaseous samples collected after 5 min from the hybrid (IOR||HER) and traditional (OER||HER) water electrolysis systems which are held at a cell voltage of 1.15 V.

Table S1. Comparison of the present study with the previously reported works for IOR (Three-electrode setup)

| S. No | Catalyst | Electrolyte | Conc. NaI (M) | V (vs RHE) @10 mA/cm$^2$ | References (DOI) |
|---|---|---|---|---|---|
| 1 | RuSn SAO | 0.1 M $HClO_4$ | 0.1 | 1.01 | 10.1021/acssuschemeng.1c01867 |
| 2 | RuTiO-550 | 0.1 M $HClO_4$ | 0.1 | 1.01 | 10.1016/j.apcatb.2022.121608 |
| 3 | RuTiO-550 | 0.1 M NaOH | 0.1 | 1.29 | 10.1016/j.apcatb.2022.121608 |
| 4 | Ni-$Co(OH)_2$ NSAs | 1 M KOH | 0.33 | 1.30 | 10.1039/D0NA00847H |
| 5 | CFP | 0.1 M $HClO_4$ | 1 | 0.55 | 10.1039/d2ta06517g |
| 6 | MS 500/CP | 0.5 M $H_2SO_4$ | 0.1 | 0.63 | 10.1002/cey2.366 |
| 7 | Mo-$N_4$/d-C | 0.1 M $HClO_4$ | 0.1 | 0.77 | 10.1021/acs.nanolett.2c01229 |
| 8 | $SO_x$-NiFeOOH | 1 M KOH | 0.33 M KI | 1.28 | 10.1039/D3CC04833K |
| 9 | $Se_x$-NiTe/NF | 1 M KOH + 0.5 M NaCl | 0.5 M KI | 1.376 (@ 100 mA/cm2) | 10.1039/D3TA04387H |
| 10 | **FTO** | **0.1 M $HClO_4$** | **1 M** | **1.04** | **Present Study** |

Table S2. Comparison of the present study with the previously reported works for IOR (Two electrode-electrolyzer setup)

| S.No | Electrocatalysts | Anolyte | Cell voltage V @ 10mA/cm$^2$ | References (doi) |
|---|---|---|---|---|
| 1. | MS 500/CP ‖ Pt@C/CP | 0.5 M $H_2SO_4$ + 0.1 M KI | 0.73 V | 10.1002/cey2.366 |
| 2. | RuSn SAO ‖ Pt/C | 0.1 M $HClO_4$ + 0.1 M NaI | 1.07 V | 10.1021/acssuschemeng.1c01867 |
| 3. | RuTiO ‖ Pt/C | 0.1 M $HClO_4$ + 0.1 M NaI | 1.09 V | 10.1016/j.apcatb.2022.121608 |
| | | 0.1 M NaOH + 0.1 M NaI | 1.30 V | |
| 4. | Ni-Co$(OH)_2$-NSAs \|\| Ni-Mo | 1 M KOH + 0.33 M KI | 1.34 V | 10.1039/D0NA00847H |
| 5. | $(SO_x)$-NiFeOOH \|\| $Ni_2P$ | 1 M KOH + 0.33 M KI | 1.36 V | 10.1039/D3CC04833K |
| 6. | $Se_x$-NiTe/NF \|\| Ni-P/NF | 1 M KOH + 0.5 M KI | ~1.64 V (@ 100 mA/cm2) | 10.1039/D3TA04387H |
| 7. | **FTO ‖ Pt-wire** | **0.1 M $HClO_4$ + 1 M NaI** | **1.15 V** | **Present study** |

References:


1. K. Gossen, and A. Ehrmann, Optik, 2019, **183**, 253-256
2. E. Hu, Y. Yao, Y. Chen, Y. Cui, Z. Wang and G. Qian, Nanoscale advances, 2021, **3**, 604-610.
3. L. Zeng, W. Chen, Q. Zhang, S. Xu, W. Zhang, F. Lv, Q. Huang, S. Wang, K. Yin, M. Li, Y. Yang, L. Gu, and S. Guo, *ACS Catal.,* 2022, **12**, 11391−11401.